The Sprott B system ⊘

Ferdinand Verhulst ✉ ⓘ ; Taoufik Bakri ⓘ

Check for updates

View Online

Export Citation

Articles You May Be Interested In

The Sprott B system

View Online   Export Citation   CrossMark

Ferdinand Verhulst[1,a] (iD) and Taoufik Bakri[2,b] (iD)

AFFILIATIONS

[1] Mathematisch Instituut, P.O. Box 80.010, 508TA Utrecht, The Netherlands
[2] TNO Sustainable Urban Mobility and Safety, P.O. Box 96800, 2509 JE The Hague, The Netherlands

[a] Author to whom correspondence should be addressed: f.verhulst@uu.nl
[b] taoufik.bakri@tno.nl

ABSTRACT

We will consider a thermostatic system, Sprott B, that is a generalization of the well-known one-parameter Sprott A system. Sprott B contains an explicit periodic solution for all positive values of the parameter a. As for Sprott A, we find dissipative KAM tori associated with time-reversal symmetry and canards in dissipative systems. The exact periodic solution is characterized by an infinite number of instability intervals of the parameter. The investigation of the dynamics in these intervals shows the presence of families of stable and unstable periodic solutions, tori, and strange attractors. For large values of the control parameter a, we find non-hyperbolic slow manifolds producing violent vibrations. We discuss a generalization of the Sprott B system with related dynamics.

Published under an exclusive license by AIP Publishing. https://doi.org/10.1063/5.0212565

We formulate and analyze a thermostatic system, Sprott B, with as basis a harmonic oscillator but with a friction term that decreases and can become negative if the oscillator energy passes a threshold characterized by one free parameter a. Such systems have been used, e.g., in the statistical mechanics of chemical physics. Apart from this application, the three-dimensional autonomous system has a more general relevance in the theory of dynamical systems. As in the well-known Sprott A system, we find near the origin of phase space canards and dissipative KAM tori. The system has many other surprising aspects. First, we have an exact and simple periodic solution for all values of parameter a. Next, it turns out that there exist an infinite number of instability intervals for discrete values of a. The Mathieu equation plays a part here. Considering the dynamics in separate instability intervals, we find many different phenomena like families of stable and unstable periodic solutions, tori, crossing of stable and unstable manifolds, and chaotic attractors. For large values of a, we find slow–fast motion with non-hyperbolic slow manifolds leading to complex dynamics. We formulate a generalization of the Sprott B system containing two parameters with similar phenomena.

I. INTRODUCTION

A brief yet inspiring paper appeared in 2013,[1] which, in a sense, continues the work initiated in Ref 2. The paper lists 17 three-dimensional autonomous ODEs with linear and quadratic terms only and one parameter, they have no equilibria. The systems are dissipative and numbered NE1, ..., NE17 with one of them, called Sprott A (or NE1). Autonomous ordinary differential equations (ODEs) of dimension 3 contain primary examples of complex behavior involving bifurcations, invariant manifolds like tori, strange attractors characterized by fractal (Kaplan–Yorke) dimensions, positive and negative, and chaos. The 17 autonomous ODE's of Ref. 1 can be studied to understand more systematically the dynamics of three-dimensional systems, we call it the Jafari–Sprott–Golpayegani project. We will review some of these results in the introduction and Section II.

Two-dimensional ODE cases have still open problems but the Jordan separation theorem prohibits the emergence of complexity in the two-dimensional case.

We note that complexity results for conservative systems were developed much earlier, in particular, for 2 degrees-of-freedom systems (four dimensions), see, for instance, Ref. 3. Examples of interesting other three-dimensional systems are the Lorentz system, the Rössler system, and the Chua circuit but these systems contain equilibria and more than one free parameter. The Jafari–Sprott–Golpayegani project simplifies the equations as much as possible.

The evidence for chaos in the 17 systems of Ref. 1 is mainly numerical but it is an important start. Strong evidence in Refs. 4 and 5 has shown that in the Sprott A system which is dissipative

families of tori arise; this is remarkable. It has been shown in Ref. 6 that these families are caused by certain symmetries of the system. Moreover, the Laskar algorithm[7] was used in Ref. 6 to demonstrate the presence of chaos between the tori in the Sprott A system.

It is of interest that the Sprott A system (NE1) arose in a slightly different form in Chemical Physics as Nosé–Hoover oscillator with thermostatic control. The motivation for studying such oscillators arises from the fact that, when using harmonic oscillators to describe the dynamics of molecular systems, the issue of non-ergodicity occurs, that is, there is no exchange of energy between particles. For further details, see Ref. 8. For the thermostatic effects, one adds in Nosé–Hoover oscillators coupling and control of energy content of the particles; this changes and stabilizes the distribution function in phase space. See Ref. 8 for an introduction and the original references.

We will make a new and interesting modification of the Sprott A system, called Sprott B. The Sprott B system has no critical points (equilibria) but an explicitly known periodic solution for all positive values of the parameter. Sprott B shows slightly stronger thermostatic effects and more complexity than the Sprott A system. It has also the advantage from a physical point of view that it directly targets the energy of the system. The presence of an explicitly known periodic solution enables us to discover many more nonlinear dynamics phenomena.

A. Setup of the paper

In Sec. II, we briefly review the results for the Sprott A system. We formulate the Sprott B system and show that it satisfies the same symmetry conditions as the Sprott A system leading to an organizing center in the form of a periodic solution surrounded by an infinite number of invariant tori. Sprott B contains a simple-looking periodic solution for all values of the threshold parameter a.

In Sec. III, linearization of the flow near the periodic solution shows the presence of an infinite number of instability segments in the parameter space of a and corresponding instability Mathieu tongues.

As expected from the symmetry established in Sec. II, we find in Sec. IV canard behavior of the solutions that approach the z axis closely. In this aspect systems, Sprott A and Sprott B are locally similar.

In Sec. V, the dynamics in the first instability tongues is explored. Using Poincaré maps, we locate periodic solutions with bifurcations. Intersection of stable and unstable manifolds produce chaos and strange attractors characterized by fractal dimensions. Several homoclinic tangles can be identified.

The bifurcation analysis is extended in Sec. VI for larger values of the parameter a. This turns out to produce many bifurcational phenomena. As an example, the case $a = 100$ is explored.

Sections VII and VIII give preliminary results for a generalization to a system with two parameters, A and B. Formally, this generalization, containing two parameters, does not fit in the Jafari–Sprott–Golpayegani project but fixing the value of A or B does. The reason to include this preliminary version here is that we expect interesting applications from the Sprott AB system, for instance, in mathematical biology.

The asymptotic analysis is usefully combined with the tools AUTO[9] and MATCONT[10] using ode78 under MATLAB and C.

II. THE SPROTT A AND SPROTT B SYSTEMS

We will briefly summarize some aspects of the Sprott A system. In Sec. II B, we will introduce the Sprott B system.

A. The Sprott A system

We formulate the equations for the Sprott A system, also known as NE1,

$$\dot{x} = y, \; \dot{y} = -x - yz, \; \dot{z} = y^2 - a, \tag{1}$$

with parameter $a > 0$. Differentiating the equation for x, we find

$$\ddot{x} + z\dot{x} + x = 0, \dot{z} = \dot{x}^2 - a, \tag{2}$$

an oscillator with variable friction and reminiscent in that sense of self-excited oscillations; however, the dynamics is very different. It was shown in Ref. 6 that in this dissipative system, an infinite number of tori are present that is caused by symmetries of the system. It is discussed with other physical examples in Ref. 11 (also see Refs. 12 and 13 for the time-reversal background). An interesting aspect of the Sprott A system but also NE9 is the observed presence of families of invariant tori, known from conservative systems but it is remarkable that we have here dissipative systems with a small parameter. This aspect was studied in more detail for Sprott A in Refs. 4 and 5 who correctly observe that we have a kind of KAM tori, see for KAM theory;[3] the evidence is numerical, see for a Poincaré map of the orbits of the Sprott A system near the origin [Fig. 1 (left)].

A novel result in Ref. 6 is that we can complete the theoretical picture for Sprott A (and NE9) by linking the tori bifurcation phenomenon to time-reversal and canards. For the Sprott A system, unbounded solutions can only be found on the z axis.

B. The Sprott B system

Consider the system,

$$\dot{x} = y, \; \dot{y} = -x - yz, \; \dot{z} = x^2 + y^2 - a, \tag{3}$$

with $a > 0$. We call system (3) as Sprott B. The Sprott B system describes again an oscillator with variable friction. Its thermostatic effect arises from the equation for z. If the action $\frac{1}{2}(x^2 + \dot{x}^2)$ is larger than $a/2$, then the oscillations described by the system for (x, y) are damped; if the action is smaller than $a/2$, then the system is excited.

As for the Sprott A system, we have that for system (3) with $a > 0$, the z axis is an invariant manifold with unbounded solutions $x = y = 0, z(t) = z(0) - at$. An interesting discrete symmetry feature of (1) was formulated in Ref. 6. It also holds for Sprott B system (3). Sprott B is a special case of the generalized Sprott AB system that will be discussed later on. We formulate the equations for the Sprott AB system and give some interesting properties in terms of hidden symmetries,

$$\dot{x} = y, \; \dot{y} = -x - yz, \; \dot{z} = Ax^2 + By^2 - a, \tag{4}$$

with $a > 0$. A, B are fixed constants.

1. Discrete symmetry

If $(x(t), y(t), z(t))$ is a solution of system (4), then $(-x(t), -y(t), z(t))$ is also a solution.
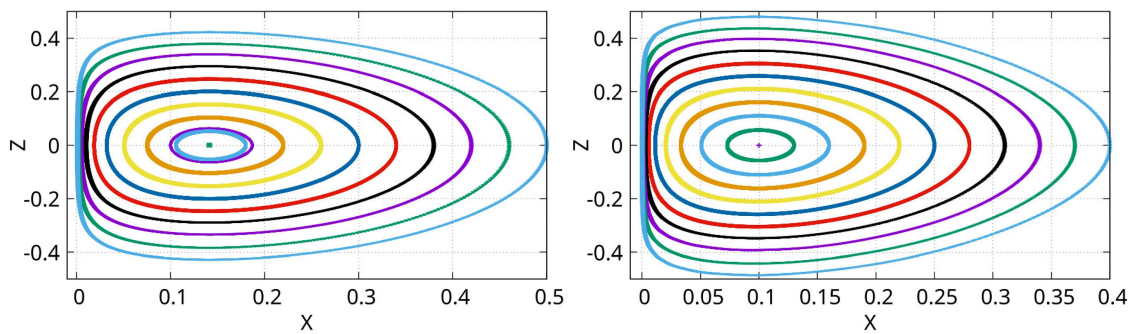
FIG. 1. Poincaré map projected onto the plane $y = 0$ of Sprott B system (1) (left, in the terminology of Sec. VII, $A = 0, B = 1$) and right, Sprott B system (3) with $A = 1$, $B = 1$ near the origin of phase space for $a = 0.01$. In both cases, the behavior near the z axis shows canard behavior for various initial conditions.

This is verified by substitution. An important feature involving time reversal of (4) is:

2. Time-reversal symmetry of Sprott B

If $(x(t), y(t), z(t))$ is a solution of system (4), then by putting $\bar{x} = x, \bar{y} = -y, \bar{z} = -z$ and reversing time $\tau = -t$, $(\bar{x}(\tau), \bar{y}(\tau), \bar{z}(\tau))$ is a solution.

Such time-reversal symmetry is called R-symmetry in Ref. 13.

Near the origin of phase space, a Poincaré map of the orbits is depicted in Fig. 1.

C. An explicit periodic solution for Sprott B

We can formulate an explicit periodic solution about the z axis in the x, y-plane for every value of $a > 0$,

$$x(t) = \sqrt{a}\cos t, \, y(t) = -\sqrt{a}\sin t, z = 0. \tag{5}$$

We can study the stability of the periodic solution (5) by perturbing near the periodic solution and linearizing. Introduce a small parameter $\varepsilon > 0$ and consider an ε-neighborhood of the periodic solution by putting

$$x = \sqrt{a}\cos t + \varepsilon X, y = -\sqrt{a}\sin t + \varepsilon Y, z = \varepsilon Z.$$

System (3) transforms to

$$\begin{cases} \dot{X} = Y, \\ \dot{Y} = -X + \sqrt{a}Z\sin t - \varepsilon YZ, \\ \dot{Z} = 2\sqrt{a}(X\cos t - Y\sin t) + \varepsilon(X^2 + Y^2). \end{cases} \tag{6}$$

The periodic matrix of the linearized system has trace 0 which corresponds to the sum of the corresponding Floquet exponents. Linearization near a periodic solution in an autonomous system produces at least one characteristic exponent 0, so we have for the remaining two exponents λ_1, λ_2,

$$\lambda_1 + \lambda_2 = 0.$$

We conclude that there is either Lyapunov stability in linear approximation (exponents imaginary) or instability with real exponents $\lambda_1 = -\lambda_2$.

We will show that an infinite number of values of a exist that lead to instability of the periodic solution. Consider system (6) and differentiate the equation for Z,

$$\ddot{Z} = 2\sqrt{a}(\dot{X}\cos t - X\sin t - \dot{Y}\sin t - Y\cos t) + O(\varepsilon).$$

Using the first two equations of (6) and assuming $a = O(1)$ yields

$$\ddot{Z} = -2a\sin^2 tZ + O(\varepsilon)$$

or

$$\ddot{Z} + a(1 - \cos 2t)Z = O(\varepsilon), \tag{7}$$

and after dividing by a and introducing a new time scale $\tau = \sqrt{a}\, t$,

$$\frac{d^2Z}{d\tau^2} + \left(1 - \cos\left(\frac{2}{\sqrt{a}}\tau\right)\right)Z = O(\varepsilon). \tag{8}$$

The linear part of the equation is the Mathieu equation that contains an infinite number of instabilities of the trivial solution at an infinite number of a values. The instabilities are found in so-called instability Mathieu tongues and are located in an infinite number of discrete segments of a values. Experimentally, we found, for instance, instability in the segment $0.658 \le a \le 1.800$ with the initial values of Fig. 3. As the eigenvalues at the instabilities are real, the nonlinear terms do not change the stability character but will produce only small quantitative changes.
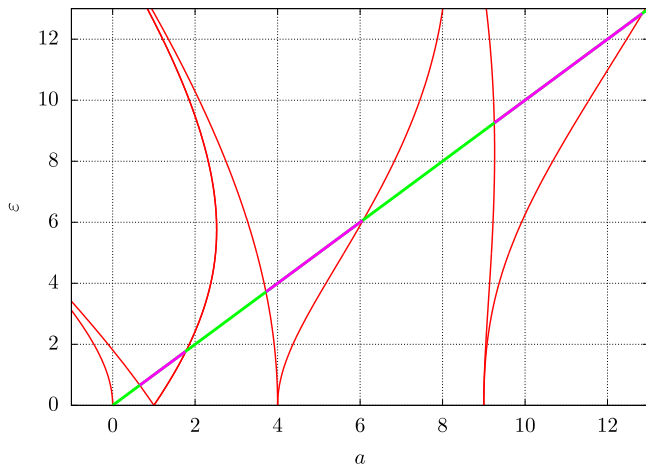
III. INSTABILITY SEGMENTS AND MATHIEU TONGUES

The Mathieu equation appears in the literature in various forms. One of the commonly used forms is

$$\ddot{y} + (a - \varepsilon\cos 2t)y = 0. \tag{9}$$

Equation (7) is just a special case of the perturbed Mathieu equation. Here, it is further required that the parameters a and ε are equal. A sufficient condition for instability is to choose the parameter a in Eq. (7) such that the point (a, a) falls within the instability regions of the Ince–Strutt diagram of the Mathieu equation (see Fig. 2).

Determining the intervals in the instability tongues involves finding the intersection points between the straight line and the corresponding Mathieu tongues of the same order. Numerical calculations of these intersection points yield the following results for

FIG. 2. Instability tongues of the Mathieu equation, with tongue boundaries corresponding to periodic solutions. The green straight line represents $\varepsilon = a$, along which we move when considering Eq. (7). The magenta segments within the unstable tongue regions indicate the unstable intervals for the parameter a. This ensures instability behavior; outside the tongues, stability is maintained. Whether the segments of the green line within the stable regions result in stability or instability of specific solutions depends on the nonlinear part and requires further investigation.

the unstable intervals with respect to the parameter a. For the first three intervals, we obtain

$$I_1 = [0.6580, 1.7796], \quad I_2 = [3.7164, 6.0782], \quad \text{and}$$

$$I_3 = [9.2539, 12.8517].$$

Additional intervals I_n for $n \in \mathbb{N}_{>3}$ can also be determined numerically.

The argument using Mathieu equation (8) does not longer hold when $a \neq O(1)$. For $0 < a \ll 1$, we will perform approximation by averaging. This has the advantage of determining also the stability for this case. Consider an ε-neighborhood of the origin of phase

space and assume $a = \varepsilon^2 a_0$ with positive a_0. Rescaling Eq. (3) by $(x, y, z) \mapsto \varepsilon(x, y, z)$ yields

$$\dot{x} = y, \quad \dot{y} = -x - \varepsilon yz, \quad \dot{z} = \varepsilon(x^2 + y^2 - a_0). \tag{10}$$

Introducing amplitude-phase transformation $(x, y) \mapsto (r, \phi)$ by $x = r\cos(t + \phi), y = -r\sin(t + \phi)$, we find from system (10),

$$\begin{cases} \dot{r} = -\varepsilon \sin^2(t + \phi)rz, \\ \dot{\phi} = -\varepsilon \sin(t + \phi)\cos(t + \phi)z, \\ \dot{z} = \varepsilon(r^2 - a_0). \end{cases} \tag{11}$$

Averaging over t and keeping the same notation for the variables, we find to $O(\varepsilon)$,

$$\dot{r} = -\varepsilon\frac{1}{2}rz, \dot{\phi} = 0, \dot{z} = \varepsilon(r^2 - a_0). \tag{12}$$

The point $r = \sqrt{a_0}, \phi = \phi_0, z = 0$ is a critical point of the averaged equations. The rank of the linearized vector field at the critical point is 2, so it follows from the 2nd Bogoliubov theorem that in an ε-neighborhood of this point, a 2π-periodic solution exists. We knew this already, it is of the form $x = \varepsilon\sqrt{a_0}\cos t$, $y = -\varepsilon\sqrt{a_0}\sin t, z = 0$; but, moreover, we know that the stability of the periodic solution is inherited by the stability of the critical point. For the theoretical background of these statements, see Ref. 14 or Ref. 15. We find purely imaginary eigenvalues and conclude that the periodic solution is Lyapunov stable. Higher order approximations in ε cannot change this as moving of the eigenvalues into the complex domain needs more dimensions.

In the sections after Sec. IV, we present analysis and a few numerical experiments to demonstrate the dynamics of Sprott B system (3) in the first instability segments. We will start close to the periodic solutions on the tongues boundaries. In Fig. 3, we show stable and unstable behavior for values of a near 0.65 and 9.2. We have plotted $R(t) = \sqrt{X^2 + Y^2 + Z^2}$. Instability intervals are for $a \in [0.658\,01, 1.779\,64]$ and $[3.716\,42, 6.078\,15]$. Figure 4 shows projections $r(t), z(t)$ of the dynamics near the stable and unstable solutions.

(a)

(b)
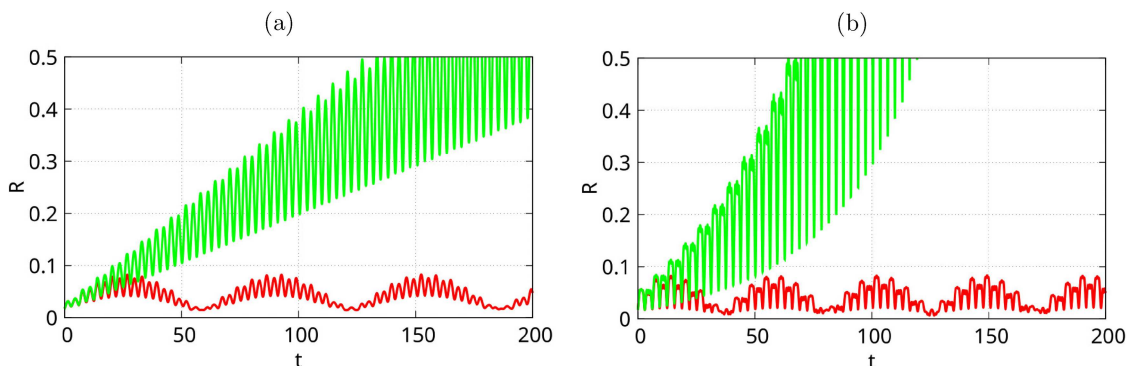
FIG. 3. Solutions $R(t)$ of Sprott B system (6) for values of a near 0.65 and 9.2 starting close to the periodic solution (5). Left (a), the case $a = 0.650$ (stable, red) and $a = 0.658$ (unstable, green). Right (b), the case $a = 9.20$ (stable, red) and $a = 9.26$ (unstable, green).
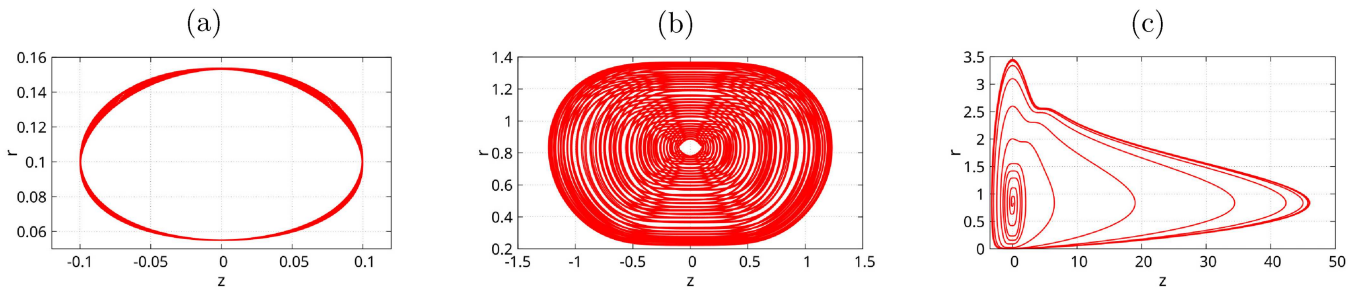
FIG. 4. Solutions $r(t), z(t)$ of Sprott B system (3) near the explicit periodic solution. (a) The case near the origin $a = 0.01, x(0) = \sqrt{a} = 0.1, y(0) = 0, z(0) = 0.1$. (b) The unstable case $a = 0.695, x(0) = \sqrt{0.695}, y(0) = 0, z(0) = 0.1$. (c) The unstable case $a = 0.7, x(0) = \sqrt{0.7}, y(0) = 0, z(0) = 0.1$.

IV. CANARD BEHAVIOR OF SPROTT B NEAR THE z-AXIS

In Sprott B system (3), we consider small values of a by putting $a = \varepsilon a_0$ (a_0 positive) and a neighborhood of the z axis by rescaling $(x.y) \mapsto \sqrt{\varepsilon}(x, y)$ resulting in

$$\dot{x} = y, \quad \dot{y} = -x - yz, \quad \dot{z} = \varepsilon(x^2 + y^2 - a_0). \quad (13)$$

This is a slow–fast system with fast moving $x(t), y(t)$ and slow $z(t)$; a slow manifold M_0 is given by $y = 0, -x - yz = 0$, corresponding with the z axis. M_0 is normally hyperbolic except close to the origin $x = y = z = 0$. The dynamics resembles the behavior of the Sprott A system near the z axis, see Ref. 6, for the theoretical background of slow–fast systems and canards, see Ref. 16. Starting with $z(0) > 0$, the solutions $x(t), y(t)$ are strongly damped and approach M_0. At some time, we have $\dot{z} < 0$ as $\dot{z}$ will be dominated by a_0, we have passed the origin and x, y will increase again. However, the increase is delayed by canard behavior. Because of the discrete symmetry of system (13) formulated in Sec. II B, the solutions $x(t), y(t)$ will show symmetric behavior near the z axis, see Fig. 5.

As in the case of the Sprott A system in Ref. 6, we find a family of tori in three-space with the periodic solution with amplitude $\sqrt{a}$ obtained before as organizing center. This is based on the time-reversal property formulated in Sec. II B.

Note that the organizing periodic solution is located at $O(\sqrt{\varepsilon})$ distance from the origin, the orbits on the tori approach the z axis exponentially close.

A more detailed analysis is given later on for possible canards in the Sprott AB system, see Sec. VIII.

V. DYNAMICS IN THE FIRST INSTABILITY SEGMENT I_1

We expect interesting dynamics when selecting the parameter a such that the periodic solution (5) becomes unstable. From the infinite number of possible cases, consider the segment $I_1 = [0.6580, 1.7796]$, the first magenta segment as depicted in Fig. 2. Tracking periodic orbits and analyzing their stability using continuation methods is crucial for detecting bifurcations and understanding the resulting dynamics and routes to chaos in the system under investigation. One of the most straightforward techniques for identifying periodic orbits in ordinary differential equations (ODEs) involves locating the fixed points of the corresponding Poincaré

return map $P(x)$. When searching for periodic orbits, if the initial guess is sufficiently close, the Poincaré return map will be well-defined. For period-1 orbits, the map exhibits a fixed point x_0 precisely at the periodic orbit. Finding this fixed point x_0 corresponds to solving the equation $P(x) - x = 0$. The Newton method is highly efficient for this task, providing an advantage as it can track periodic orbits regardless of their stability. However, the Poincaré return map is typically not available in an analytical form and must be computed numerically. Additionally, the Newton method requires both the map $P(x)$ and its first derivative $DP(x)$. Mastery of the numerical computation of the Poincaré map and its derivative is essential. For more detailed expressions, including second-order derivatives of the Poincaré map, refer to Ref. 17. In Sec. V A, we demonstrate the efficiency of this method in identifying short periodic orbits through a single return step within the Mathieu tongues under study. Periodic orbits are crucial for comprehending the complex dynamics induced by non-linearities and detecting chaotic behavior in the dynamical system via bifurcation analysis. Applying the fixed point approach to
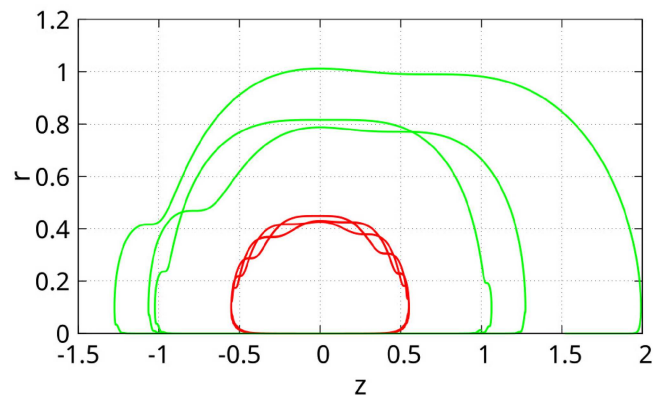
FIG. 5. Two canard solutions $r(t), z(t)$ near the z axis located on tori of Sprott B system (3) with $r = \sqrt{x^2 + y^2}$. We have $a = 0.01$ and near the z axis, $x(0) = y(0) = 0.01$. For $z(0)$ the cases, $z(0) = 0.5$ (red curve) and $z(0) = 1$ (green curve). The solutions are not periodic and show symmetric canard behavior near the z axis that is close to the slow manifold of the slow–fast system.
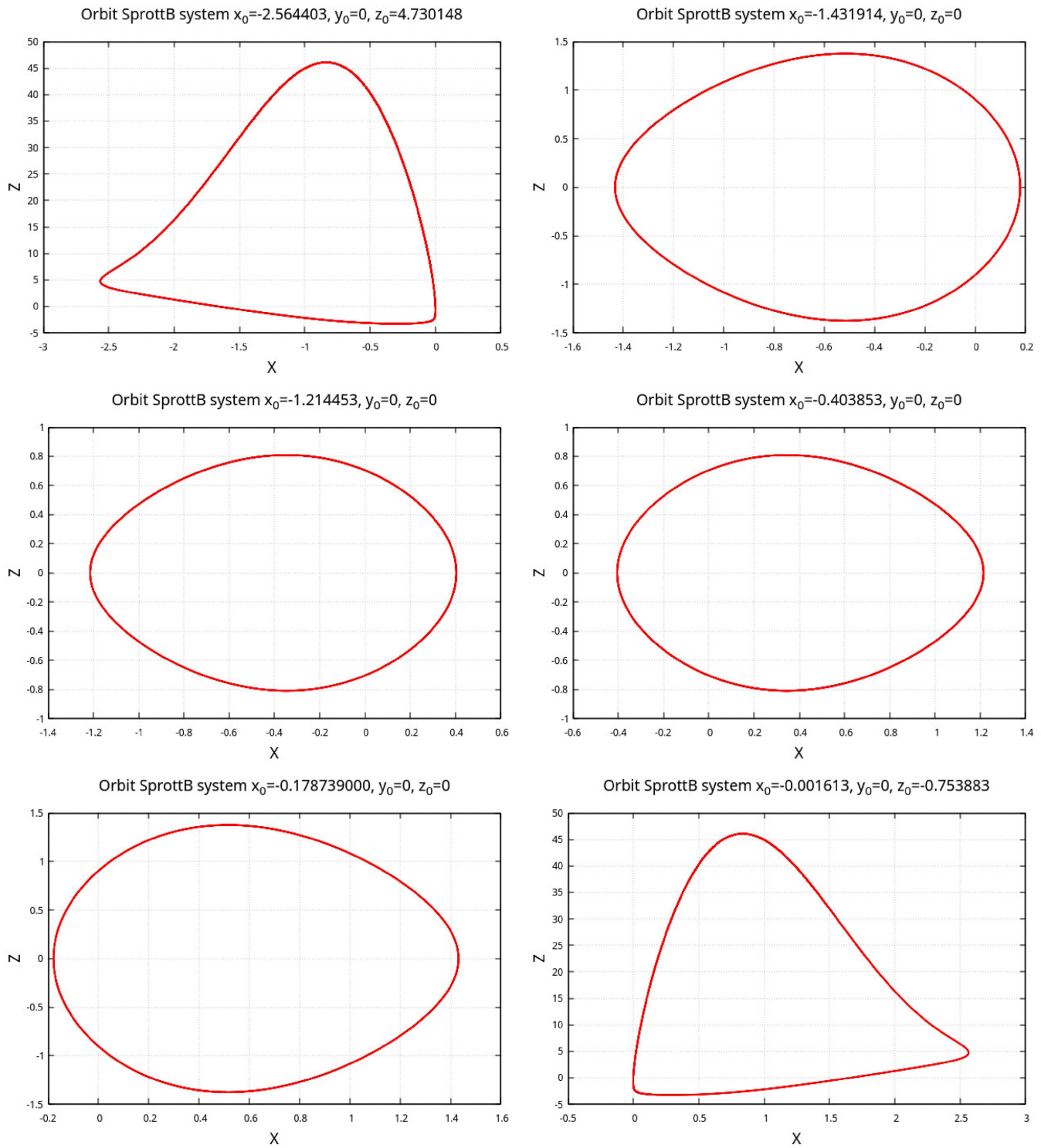
FIG. 6. All six additional periodic orbits from Table I numerically detected via the computation of the fixed points of the Poincaré return map in the case $a = 0.698\,11$. The periodic orbits related by the discrete symmetry can easily be identified.

TABLE I. List of all the periodic orbits numerically detected using the Poincaré map fixed point approach for $a = 0.698\,11$. Orbit 4 corresponds with the explicit periodic orbit discussed previously. Orbits (1,7); (2,6); and (3,5); respectively; are related through the discrete symmetry. Time-reversal symmetric periodic orbits can be inferred from these seven periodic solutions using the time-reversal property of system (4) discussed earlier.

Orbit	x_0	y_0	z_0	Period	Comment
1	$-2.564\,403$	$0.000\,000$	$4.730\,148$	125.935	Stable (node)
2	$-1.431\,914$	$0.000\,000$	$0.000\,000$	8.057	Unstable (saddle)
3	$-1.214\,453$	$0.000\,000$	$0.000\,000$	6.778	Stable (focus)
4	$-0.835\,529$	$0.000\,000$	$0.000\,000$	2π	Unstable (saddle)
5	$-0.403\,853$	$0.000\,000$	$0.000\,000$	6.778	Stable (focus)
6	$-0.178\,739$	$0.000\,000$	$0.000\,000$	8.057	Unstable (saddle)
7	$-0.001\,613$	$0.000\,000$	$-0.753\,883$	125.935	Stable (node)

$P^2(x), P^3(x), \ldots, P^n(x)$ yields higher periods $2, 3, \ldots, n$ of the Sprott B system. In the instability segments $I_{1,\ldots,9}$, we focus on P^1.

A. The case $a = 0.698\,11$

Starting at the parameter value $a = 0.698\,11$ in the first instability interval I_1, we look for P^1 periodic orbits with starting values on the xz-plane. We choose x_0, z_0 within a square of side with length 4 centered around the explicit periodic orbit (5) with $(x(0), y(0), z(0)) = (\sqrt{a}, 0, 0)$, we find six additional periodic orbits, see Table I and illustrations in Fig. 6. Only three of the found periodic orbits are intrinsically different, the other three can be deduced from the symmetries in the system mentioned earlier. The periodic orbits are not detected by averaging as they do not arise as a continuation of a known periodic orbit. This is clear from the periods in Table I.

Looking at the dynamics close to the periodic orbits, we find orbits showing complex motion suggesting chaotic dynamics, see Fig. 7. Examining the Poincaré section of the system shows indeed the picture of a strange attractor, see Fig. 8. The calculation of the

Lyapunov exponents finally reveals chaotic motion as the largest Lyapunov exponent is positive,

$$\lambda_1 = 0.012\,719\,265;\ \lambda_2 = 2.807\,378\,8 \times 10^{-6};\ \lambda_3 = -0.012\,719\,288. \tag{14}$$

The manifolds shown in Figs. 7 and 8 are fractal.

Remarkably, the sum of the Lyapunov exponents is very close to zero, see Fig. 9, obviously close to being a conservative system.

B. Bifurcation analysis in the first Mathieu tongue

The explicit orbit (5) (see Table I) is continued using the software packages AUTO and MATCONT, see Fig. 10. At each of the boundaries of the first tongue, there is a branching point cycle bifurcation BPC (square symbol). Orbit 3 of the table emerges from the left BPC point as a stable cycle at the parameter value $a = 6.579\,13 \times 10^{-1}$ while orbit 4 (5) looses stability due to the BPC bifurcation and the entrance of the first Mathieu tongue. Continuation of orbit 3 yields a fold bifurcation (dianmond symbol), at the parameter value $a = 7.097\,73 \times 10^{-1}$, where orbits 3 and 2 collide and disappear. Further continuation of orbit 2 yields a high period ($T \simeq 182$) at
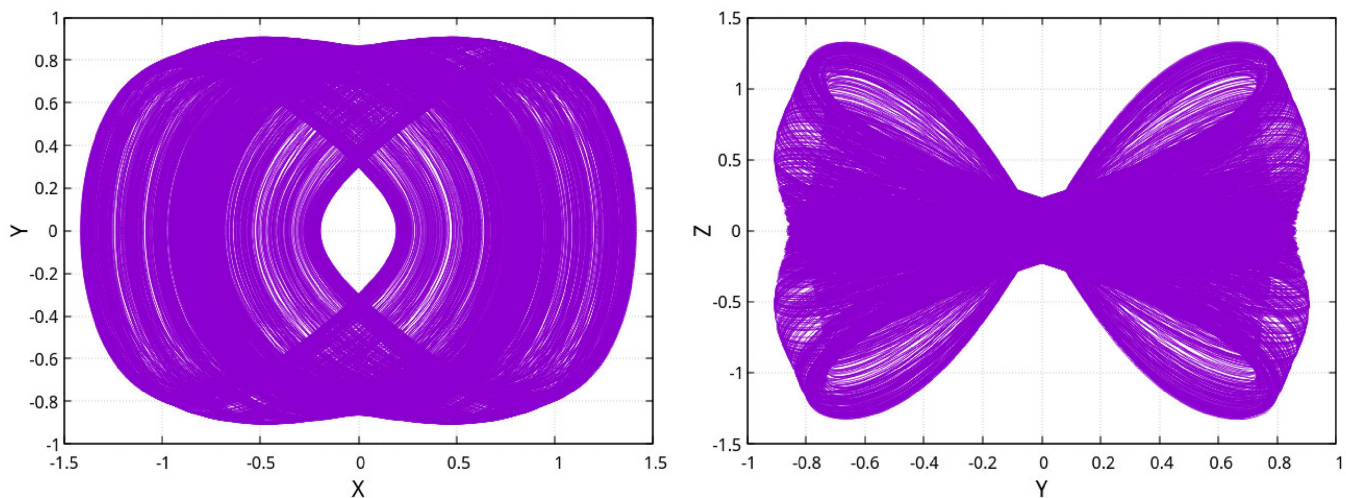
FIG. 7. Orbits of Sprott B system (6) showing chaotic motion for values of $a = 0.698\,11$ starting close to the periodic solution (5) at $x(0) = \sqrt{a}$, $y(0) = 0$, $z(0) = 0.01$.
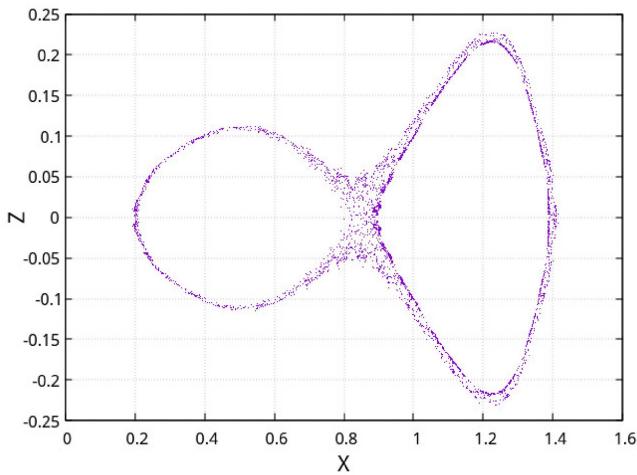
FIG. 8. Poincaré section ($y = 0$) of Sprott B system (6) showing a strange attractor for values of $a = 0.698\,11$ starting close to periodic solution (5) at $x(0) = \sqrt{a}$, $y(0) = 0$, $z(0) = 0.01$.

the value $a = 0.5$ suggesting the presence of a canard structure (see Fig. 11). Orbits 1 and 7 are not related to any of the other orbits found in Table I. They are stable within this tongue and do not undergo any bifurcation as the parameter a is varied within the first tongue. They are omitted here due to the very high periods and stable character. At the right BPC, a periodic orbit emerges that is not detected in Table I because the orbit does not exist for $a = 0.698\,11$. This stable cycle undergoes a supercritical Period-Doubling (PD) bifurcation (circle symbol) at the parameter value $a = 1.588\,27$. It looses stability to the period 2 cycle emerging from it. Further continuation of the unstable cycle yields no new bifurcations. Its period

increases rapidly and becomes $T \simeq 93$ at the parameter value $a = 1$ suggesting here also the presence of a canard structure (see Fig. 12).

1. Homoclinic tangles

One of the routes to chaos is via homoclinic tangles, this is underlying the chaos as depicted in Figs. 8 and 13 and how we numerically computed the stable and unstable manifolds of the saddle. The original idea was conceived by Poincaré and can be found in Ref. 18, vol. 3. Considering a saddle point of a Poincaré map, one can identify stable and unstable manifolds emerging from the saddle. The complexity of transversal crossing of the manifolds produces the wild behavior that nowadays is identified as chaos and horseshoe dynamics; the last geometric insight was of course still unknown in Poincaré's time.

## VI. BIFURCATION ANALYSIS WHEN CONTINUING a

Continuation of the explicit periodic solution (5) by increasing the parameter a as control parameter, we enter different instability segments. As in the case of segment I_1 the periodic solution undergoes a series of branching point bifurcations (BPCs) exactly at the Mathieu tongues boundaries that were computed above as boundaries of the intervals I_n, see Fig. 14. Here, the explicit periodic orbit looses stability and a new cycle branches from it. Figure 14 shows that the bifurcations within each tongue are quite different. There are many different cases, in what follows we will restrict ourselves to a few observations.

A. The case $a = 1$

In Fig. 15, we show the behavior of $r(t), z(t)$ with time. In Fig. 16, we show a periodic solution with canard behavior, the slow manifold $y = 0$ extends to negative values of $z(t)$.
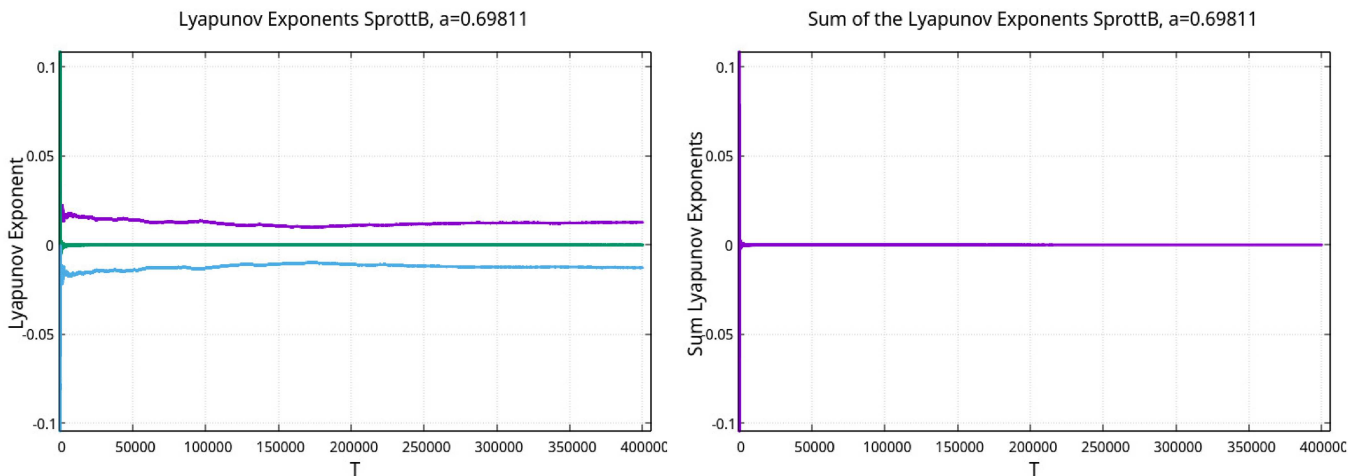
FIG. 9. Lyapunov exponents of the SprottB system for $a = 0.698\,11$ (left) and their sum (right).
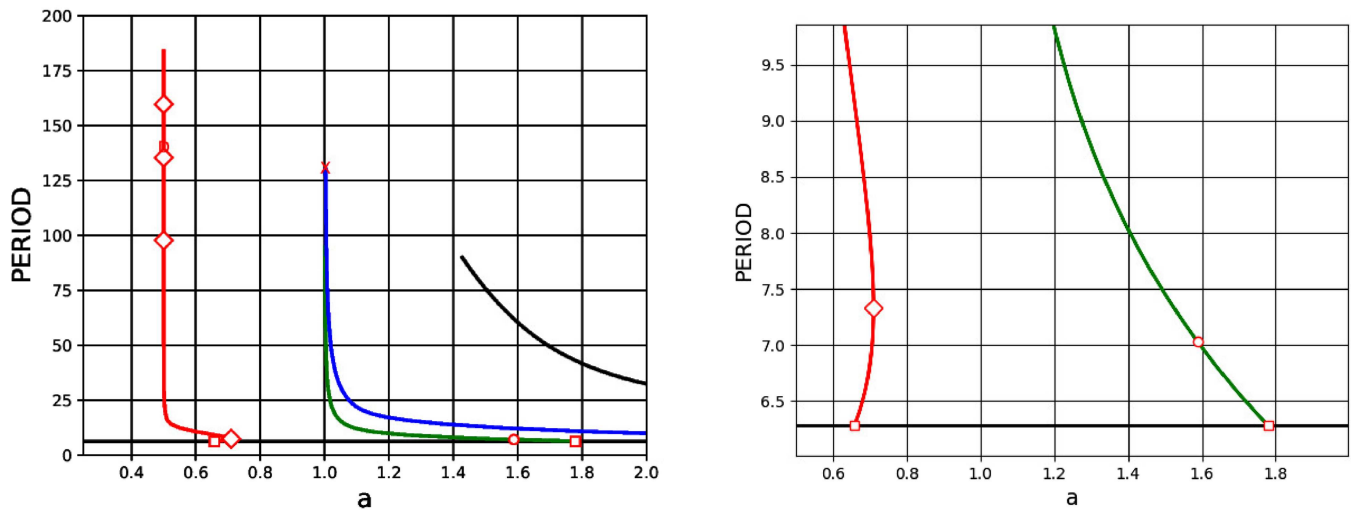
FIG. 10. Left: the bifurcation diagram of the explicit periodic orbit near the first Mathieu tongue ($a \in I_1 = [0.6580, 1.7796]$). Each curve represents a periodic orbit that bifurcates from the explicit periodic solution as the control parameter a enters the limits of the first tongue. Right: a zoomed-in view of the first tongue. A branching point cycle bifurcation (BPC) is indicated by a square symbol, a fold bifurcation by a diamond symbol, and a period-doubling (PD) bifurcation by a circle symbol. Note the asymptotic behavior of the period as the control parameter approaches 0.5 and 1. Refer to Figs. 11 and 12 for the corresponding orbits.

B. The case $a = 4$

In this case, the solutions starting near the exact unstable periodic solution tend to a stable periodic solution, see Fig. 17. As $z(t)$ assumes successively positive and negative values, this periodic solution has the character of a self-excited oscillation.

There are many interesting phenomena. We mention the periodic orbit starting at $x(0) = -1.9283478735053221$; $y(0) = 0$; and $z(0) = 0.0000000000641302$. This orbit has one multiplier 1 and two on the unit circle in the complex plane.

For larger values of a ($a = m^2$, $m \in \mathbb{N}_{\geq 3}$) at the instability intervals, we find similar phenomena.
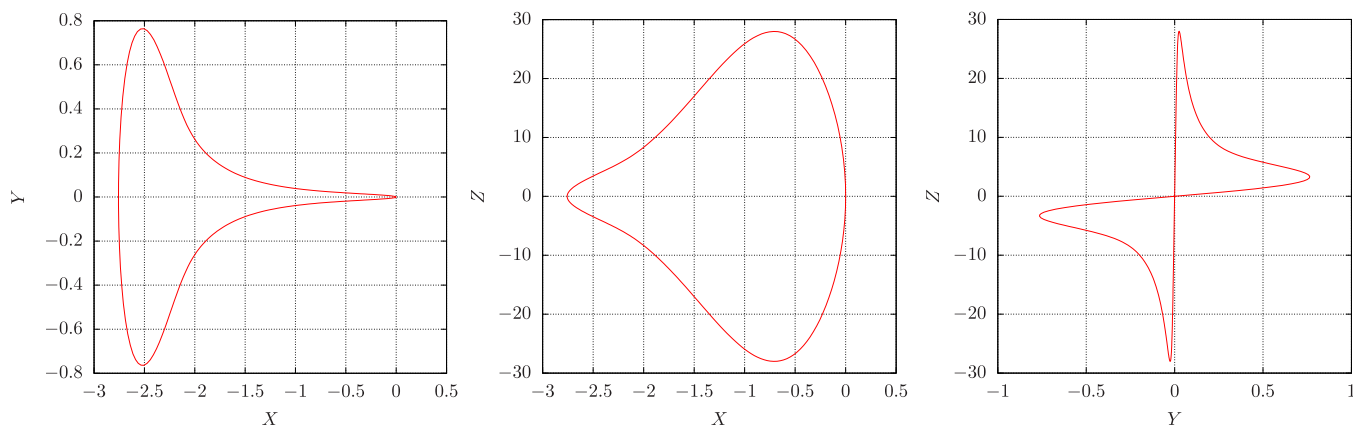
C. The case $a \gg 1$

We discuss phenomena arising for $a \gg 1$. In Fig. 18, we show the 9th and 10th instability tongues at $a = 81, 100$. Assume
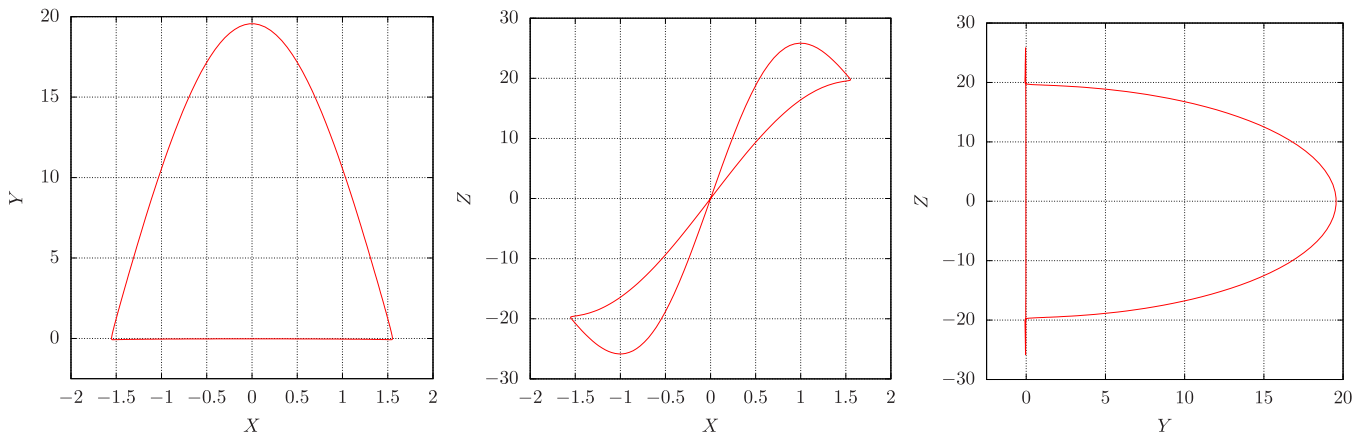
$$a = \frac{a_0^2}{\varepsilon^2},$$

with $a_0 > 0$ and ε a small, positive parameter. The periodic solution (5) becomes

$$x(t) = \frac{a_0}{\varepsilon} \cos t, \ y(t) = -\frac{a_0}{\varepsilon} \sin t, \ z = 0. \tag{15}$$

FIG. 11. Orbit 2 at the parameter value $a = 0.5$ with high period $T = 182.16$ and initial conditions: $x(0) = -1.5626736828$, $y(0) = -0.10021733463$, and $z(0) = -15.785\,176\,678$.

FIG. 12. Orbit emerging from the right hand sidebranching point at the parameter value $a = 1$ with high period $T = 93.74$ and initial conditions $x(0) = -1.2374102968$, $y(0) = 6.3677142199$, and $z(0) = -18.448\,524\,598$.

Consider a perturbation X, Y, z of the periodic solution, putting

$$x(t) = \frac{a_0}{\varepsilon} \cos t + X, y(t) = -\frac{a_0}{\varepsilon} \sin t + Y, z(0) = z_0.$$

System (3) transforms to

$$\begin{cases} \dot{X} = Y, \\ \varepsilon \dot{Y} = a_0 z \sin t - \varepsilon X - \varepsilon Yz, \\ \varepsilon \dot{z} = 2a_0(X \cos t - Y \sin t) + \varepsilon(X^2 + Y^2). \end{cases} \quad (16)$$

Slow–fast system (16) has a set of slow manifolds of the form

$$X(t) = c \sin t, Y(t) = c \cos t, z(t) = 0, \quad (17)$$

with c an arbitrary constant but small to be in a neighborhood of the periodic solution. The slow manifolds are not hyperbolic, we have a rather degenerate slow–fast system. Numerical simulations for $a = 100$ show large excursions of $z(t)$, see time series in Fig. 20. Note that for $a = 100$, the system lies within the ninth Mathieu tongue associated with $a = 81$, as depicted in Fig. 18. Numerical computation of the intersection points of the green line with the boundaries of the ninth tongue yields the interval $I_9 = [94.343, 105.346]$. Initiating just outside the ninth tongue ($a = 94$) results in a torus near the Lyapunov-stable exact periodic orbit, as shown in Fig. 19. Conversely, initiating inside the tongue confirms that the exact periodic orbit is numerically unstable, as theoretically predicted. Figure 20 presents the time series and Poincaré sections for $a = 100$ starting
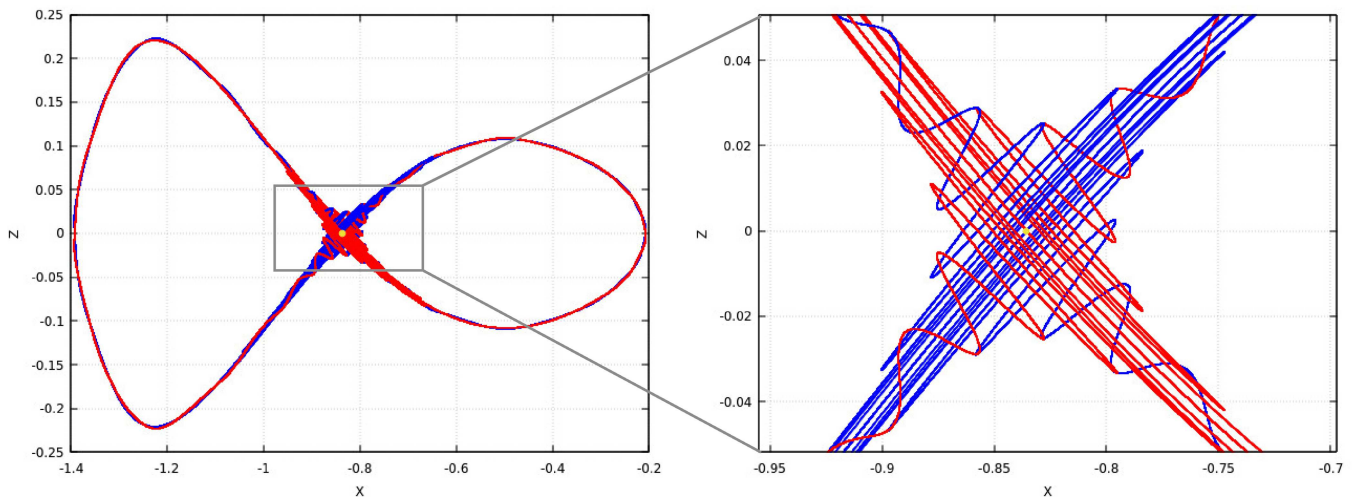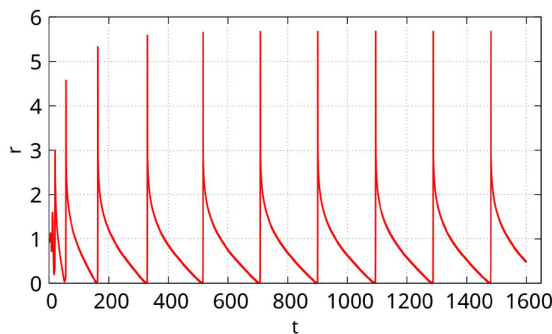

FIG. 13. 1D stable (blue) and unstable (red) manifolds of the Poincaré map of the saddle cycle intersecting transversally at the parameter value $a = 0.698\,11$. The yellow dot in the middle is the fixed point corresponding with the explicit saddle periodic orbit found before (left). Right is a blowup near the saddle showing the transversal intersection leading to homoclinic tangles and complex Horseshoe dynamics.
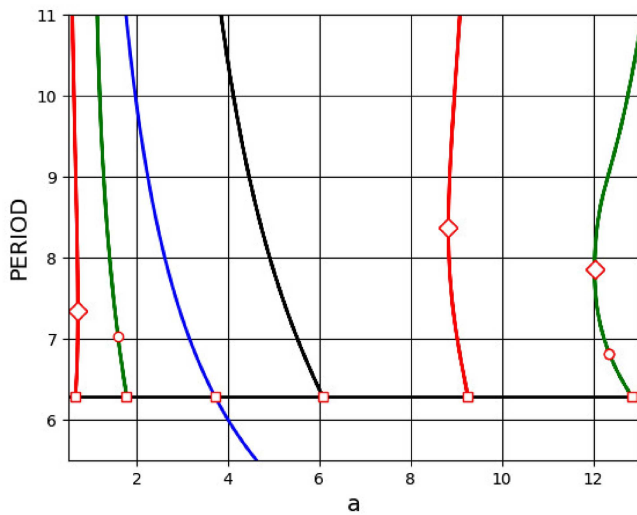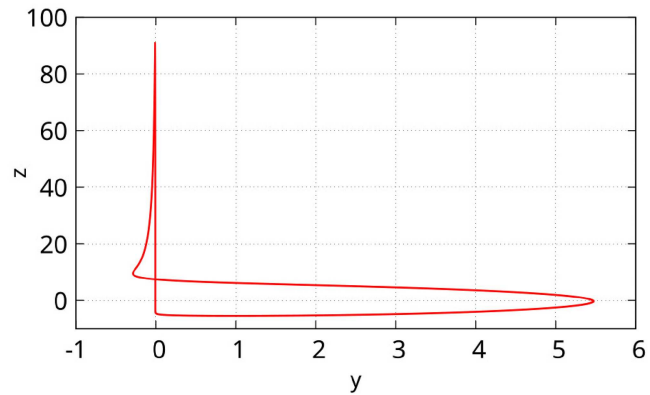
FIG. 14. Bifurcation diagram of the explicit cycle in the first three Mathieu tongues with a as control parameter. The squares correspond to the BPC, diamonds are points where a fold bifurcation takes place, and circles correspond to period-doubling bifurcations that later turn out to be a strong resonance 1:2 where a Neimark-sacker curve and a PD curve intersect with a double multiplier equal to -1.

from two sets of initial values near the unstable exact 2π-periodic solution. Conducting a detailed bifurcation analysis within the ninth Mathieu tongue would enhance the understanding of the system's dynamics.

An interesting case arises when $a = 100$, denoted as point P in Fig. 18. Here, two saddle periodic solutions exhibit a heteroclinic connection for a critical value of a close to 100. These solutions are identified as fixed points with period 2 in the Poincaré section $y = 0$ at coordinates $(x, z) = (-7.796\,65, -10.445\,12)$, shown in Fig. 21(a) as a magenta dot, and $(x, z) = (-9.111\,83, -5.891\,99)$ as a green dot. As the parameter a deviates from this critical value, the stable and unstable manifolds of one periodic solution intersect in a nontrivial, intricate manner with the stable and unstable manifold of the

FIG. 16. Projection of solution $y(t), z(t)$ of Sprott B system (3) for $a = 1$ starting close to the explicit periodic solution in (5), with initial condition $x(0) = \sqrt{a}, y(0) = 0, z(0) = 0.1$, and tending to another periodic solution with canard behavior.

other. This intersection results in heteroclinic tangles and chaotic dynamics.

VII. GENERALIZATION TO A SPROTT AB SYSTEM

We generalize the Sprott B system to Sprott AB system (4) by adding two fixed parameters A, B. The Sprott B system is included if we choose $A = B = 1$. We expect new dynamical features when choosing $A \neq B$. This section and the next one are introductory, there are many open questions for the Sprott AB system which need to be studied in more detail in the future.

For any fixed A, B values, system (4) fits in the Jafari–Sprott–Golpayegani project provided that for these values of parameters A, B chaos is present. If both A and B are negative, $z(t)$ will decrease monotonically and the dynamics will remain simple; we, therefore, exclude this case. Note that the generalized Sprott AB system reduces to the Sprott A system if $A = 0, B = 1$ and to the Sprott B system for $A = B = 1$. The case $A = B$ is strongly related to the Sprott B system, we will, therefore, consider in what follows

FIG. 15. Solutions $r(t), z(t)$ of Sprott B system (6) for values of $a = 1$ starting close to the explicit periodic solution in (5), with initial condition $x(0) = \sqrt{a}, y(0) = 0, z(0) = 0.1$.
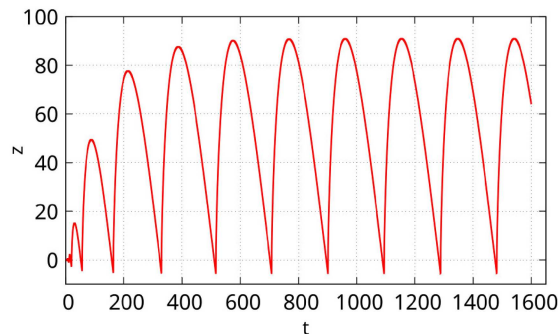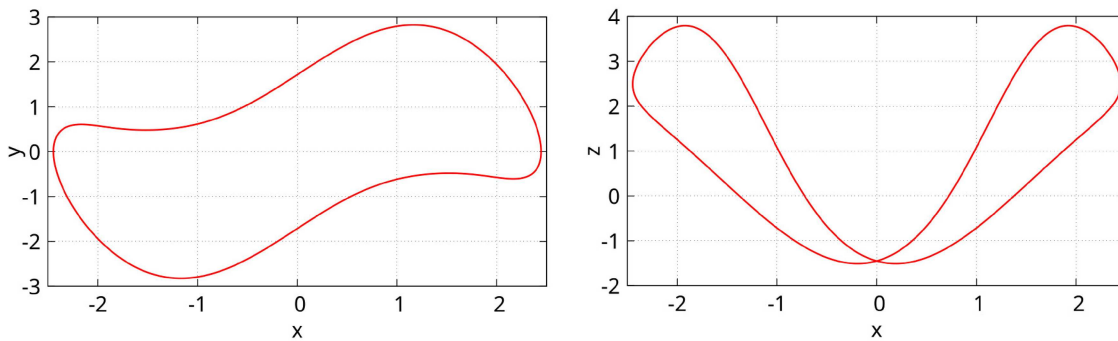
FIG. 17. Solutions $x(t), y(t)$ (left) and $x(t), z(t)$ (right) of Sprott B system (3) with $a = 4$. Starting close to the unstable periodic solution (5) [$x(0) = 2, y(0) = 0$, $z(0) = 0.001$], the solution moves to a stable periodic solution, the transitional behaviour is left out. Initial conditions $x(0) = -1.90653, y(0) = 0.549365$, and $z(0) = 3.76222$.

$A \neq B$. It turns out that near the origin of phase space, one parameter, $A + B$, plays an essential part in the dynamics. For reasons of comparison, we will choose

$$A + B = 1.$$

As for the Sprott A and Sprott B systems, we have that for arbitrary $a > 0$, the z axis is an invariant manifold with unbounded solutions $x = y = 0, z(t) = z(0) - at$.

Note that by differentiating the equation for x, we can rewrite system (4) as

$$\ddot{x} + \dot{x}z + x = 0, \quad \dot{z} = Ax^2 + B\dot{x}^2 - a. \tag{18}$$

A. A periodic solution near the origin

For the Sprott AB system with $A \neq B$, we do not have an exact periodic solution at our disposal, but for a small and near the origin, we can obtain existence and approximation of a periodic solution.
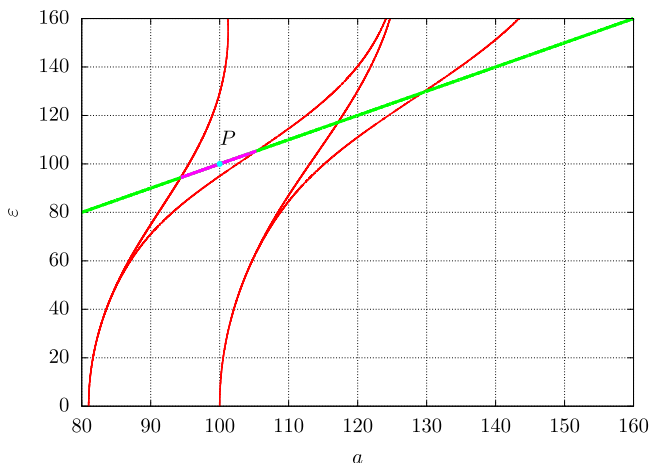
FIG. 18. 9th and 10th Mathieu stability tongues, $a \gg 1$.

Considering small values of parameter a and solutions ε-close to the origin of phase space, we transform

$$x \to \varepsilon x, y \to \varepsilon y, z \to \varepsilon z, a = \varepsilon^2 a_0, \tag{19}$$

with $a_0 > 0$ and ε a small positive parameter. System (4) becomes

$$\dot{x} = y, \quad \dot{y} = -x - \varepsilon yz, \quad \dot{z} = \varepsilon \left(Ax^2 + By^2 - a_0 \right), A + B = 1. \tag{20}$$

Transforming $(x, y) \mapsto (r, \phi)$, we use amplitude-phase coordinates $x = r\cos(t + \phi), y = -r\sin(t + \phi)$ and average over time t. For the theory of averaging, see Ref. 19; we find to first order in ε,

$$\dot{r} = -\frac{\varepsilon}{2}rz, \dot{\phi} = 0, \dot{z} = \frac{\varepsilon}{2}\left(Ar^2 + Br^2 - 2a_0 \right) = \frac{\varepsilon}{2}\left(r^2 - 2a_0 \right). \tag{21}$$

Using again the second Bogoliubov theorem (see Ref. 14), we know that a critical point of system (21) under certain implicit function conditions corresponds with a periodic solution of system (20) that is ε-close to the critical point. We find for the critical point,

$$r_c = \sqrt{\frac{2a_0}{A + B}} = \sqrt{2a_0}, \ z = 0. \tag{22}$$

If the Jacobian of the averaged system at the critical point is structurally stable, the stability of the periodic solution follows from the eigenvalues at the critical point. The eigenvalues are given by the characteristic equation,

$$\lambda(\lambda^2 + a_0) = 0.$$

Following the same reasoning as in the case of the periodic solution of the Sprott B system, we conclude Lyapunov stability of the periodic solution found by averaging.

An illustration of the dynamics near the origin of phase space is shown in Fig. 22 for $A = 0.65, B = 0.35$. The picture suggests again, at least for these values of A, B, the existence of tori and canard behavior near the z axis.

VIII. CANARD BEHAVIOR OF SPROTT AB NEAR THE z-AXIS

As before, we assume $A + B = 1$ but admit negative values of A or B. It was shown in Ref. 6 that if a is small, we have a singular
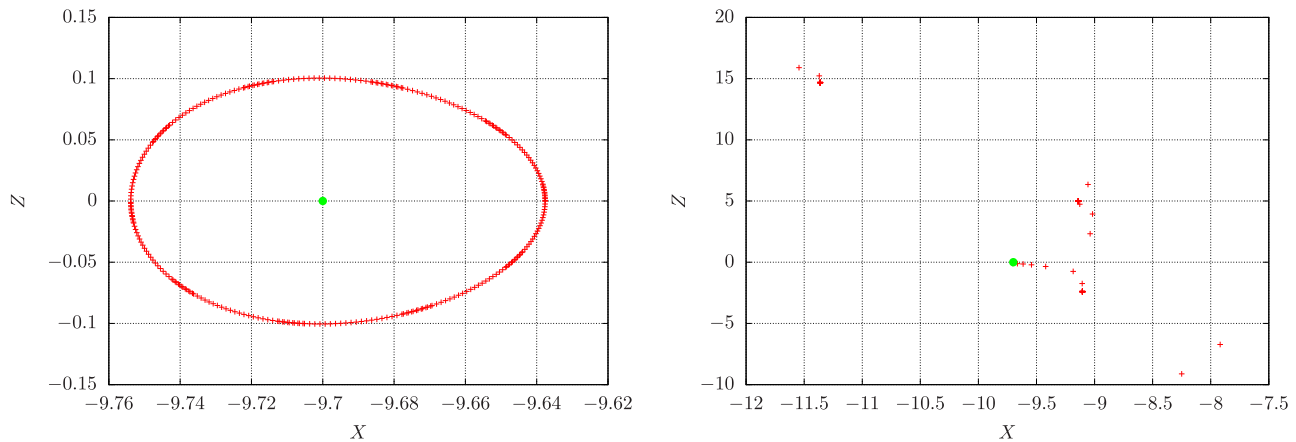
FIG. 19. Poincaré section ($y = 0$) showing a $\mathbb{T}^2$ torus of system 3 near the trivial periodic orbit with $a = 94$ outside the 9th Mathieu tongue (left). The periodic orbit is Lyapunov stable. Right the Poincaré section for $y = 0$ at $a = 94.5$ inside the 9th tongue showing the trivial periodic orbit is unstable; initial conditions for both cases are $x(0) = \sqrt{a}, y(0) = 0$, and $z = 0.1$. The green dot corresponds to the trivial periodic orbit.
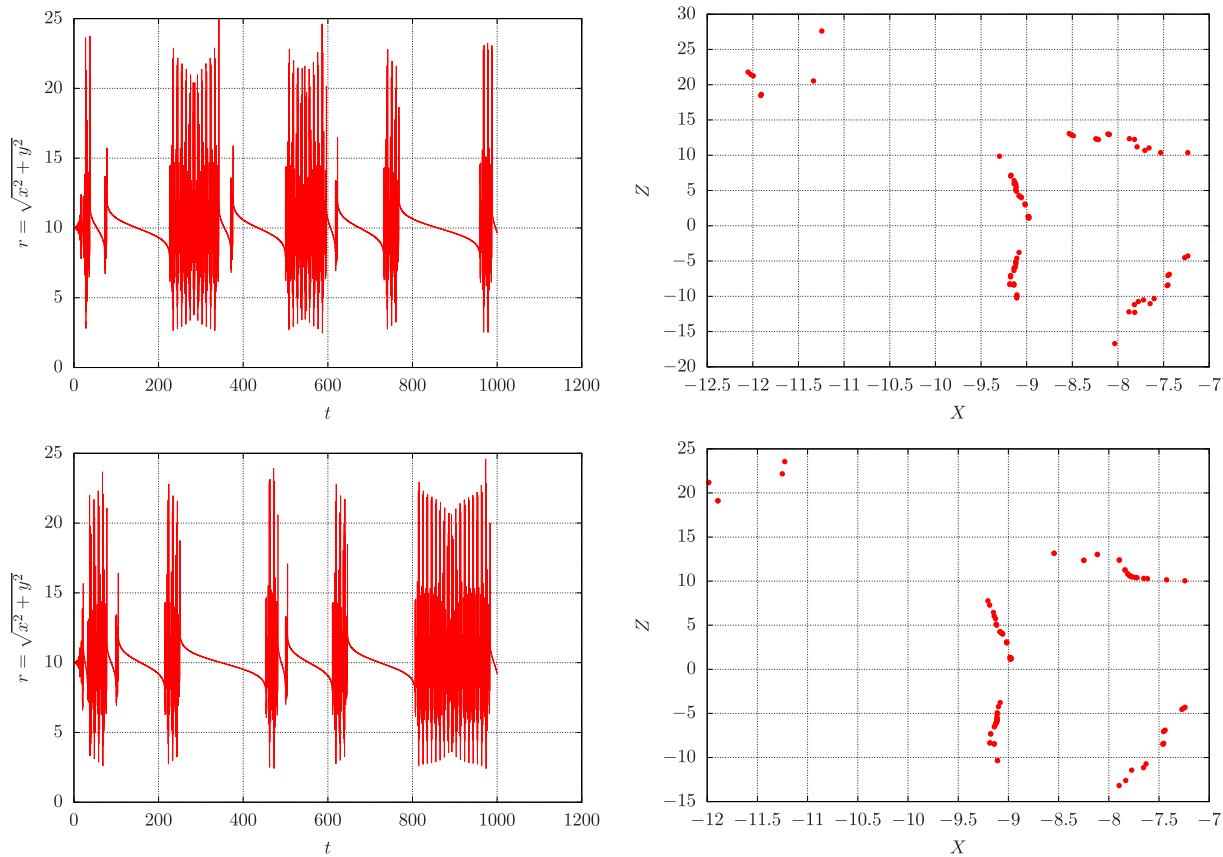
FIG. 20. Time series and Poincaré sections of the Sprott B system for $a = 100$, top initial values $x(0) = 10, y(0) = 0$, and $z(0) = 0.1$, below $x(0) = 10$, $y(0) = 0$, and $z(0) = -0.1$. The sections are at $y = 0$. The time series left show $r(t) = \sqrt{x^2 + y^2}$; strong vertical motion corresponds with the fibers around the non-hyperbolic family of slow manifolds, mildly curved lines correspond with large positive (damping) values of z. The Poincaré section right for $z(0) = \pm 0.1$ show an attractor consisting of two connected parts.
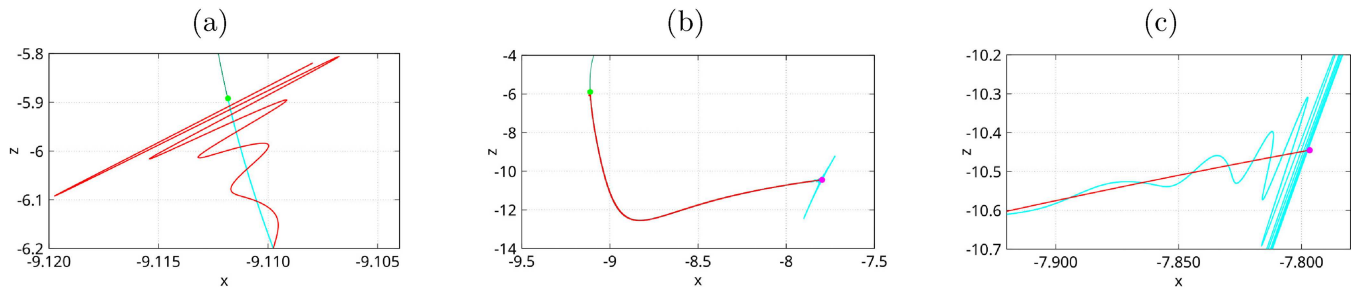
FIG. 21. Poincaré section at $y = 0$ for $a = 100$, $A = B = 1$. The figure illustrates two unstable periodic solutions with a heteroclinic connection. Panel (b) shows the overall heteroclinic connection. Panel (a) provides a zoomed-in view around the green fixed point, highlighting the intersection between the unstable manifold of the magenta dot (red curve) and the unstable manifold of the green equilibrium (cyan curve). Panel (c) depicts the dynamics in the vicinity of the magenta dot.

perturbation problem with canard behavior for Sprott A system (1). We study Sprott AB system (4) as a slow–fast system and will apply Tikhonov's theorem.[20] Note that for system (4),

$$\frac{dr^2}{dt} = -2\dot{x}^2 z,$$

so, as for the Sprott A and Sprott B systems and as long as $z(t)$ is positive, the (x, y) phase-flow is strongly damped; if $z(t)$ is negative, the flow is excited. We expect that when starting with positive $z(0)$, large enough the solution tends relatively fast to a neighborhood of $x(t), y(t) = O(\sqrt{\varepsilon})$ (near the z axis); after this, the canard behavior near the z axis will start, see Fig. 23.

To put the system in the formulation of Tikhonov's theorem, we rescale system (4) slightly differently,

$$x = \varepsilon \bar{x}, y = \varepsilon \bar{y}, a = \varepsilon a_0.$$

Omitting the bar system (4) becomes

$$\dot{x} = y, \dot{y} = -x - yz, \dot{z} = -\varepsilon a_0 + \varepsilon^2 (Ax^2 + By^2), A + B = 1. \quad (23)$$

Rescaling time $\tau = \varepsilon t$, we find the equivalent system as

$$\varepsilon \frac{dx}{d\tau} = y, \varepsilon \frac{dy}{d\tau} = -x - yz, \frac{dz}{d\tau} = -a_0 + \varepsilon(Ax^2 + By^2). \quad (24)$$

According to geometric singular perturbation theory, system (24) shows fast motion of the x, y-component in the timelike variable τ, except in an $O(\varepsilon)$ neighborhood of the one-dimensional approximate slow (or critical) manifold M_0 defined by

$$y = 0, -x - yz = 0. \quad (25)$$

The approximate slow manifold M_0 corresponds with the z axis in three-dimensional phase space, it is normally hyperbolic when excluding a neighborhood of $z = 0$ as we have for the fast part of the system that the real part of the spectrum is $-z/2$. M_0 approximates the smooth slow manifold M_ε that exists for solutions of system (24). According to Sec. 15.7 of Ref. 16, when excluding a neighborhood of $z = 0$, M_0 approximates M_ε exponentially close. To fix ideas, we take initially $x(0), y(0)$ small and $z(0) > 0$.

When starting outside M_0 at positive $z(0) = z_0$, $z(t)$ of system (24) will change little. An $O(\varepsilon)$ approximation of the fast solutions
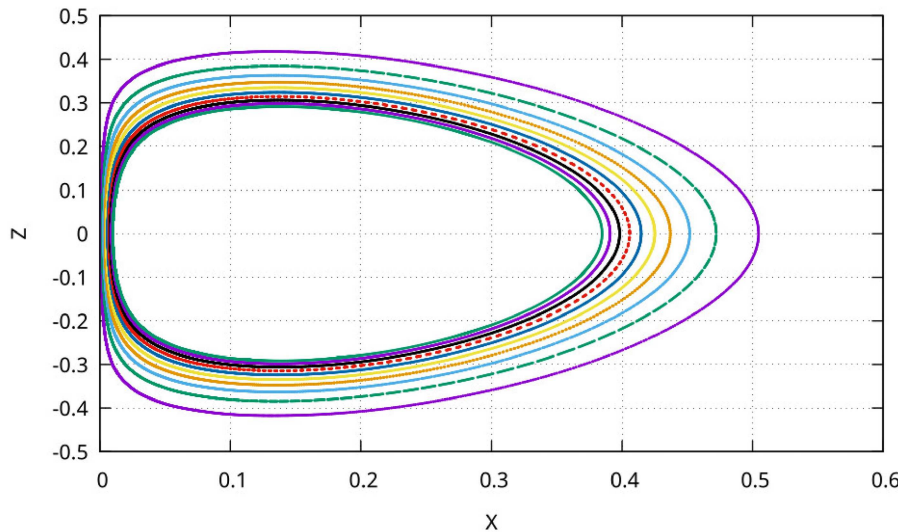
FIG. 22. Poincaré map in the plane $y = 0$ of Sprott AB system (4), for the random case $A = 0.65, B = 0.35$ near the origin of phase space, for $a = 0.01$. The behavior near the z axis shows canard behavior for various initial conditions.
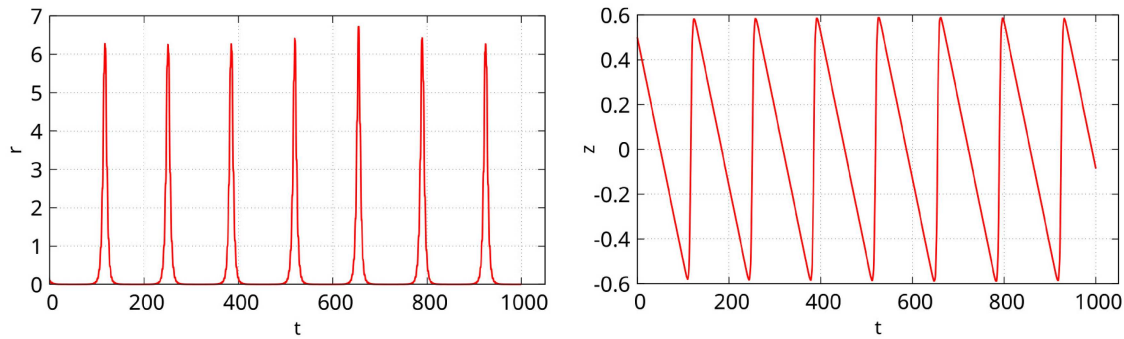
FIG. 23. Canard behavior of $r(t)$, $z(t)$ of Sprott B system (23), $A = 0.5$ and $B = 0.5$. We have $a_0 = 0.1$, $\varepsilon = 0.1$, $z(0) = 0.5$, $x(0) = 0.1$, $y(0) = 0$, and $z(t)$ alternates in sign. The value of $z(0)$ forces the $x(t)$, $y(t)$ behavior to approach the z axis in its stable part, when passing the origin, this part of the z axis becomes unstable but the motion along the axis persists for some time (canard behavior).

of the system will be of the form

$$X_0(t) = x_0 e^{-z_0 t/2} \cos\left(\sqrt{4 - z_0^2}\, \frac{t}{2}\right). \tag{26}$$

The approximation is valid on an interval $O(1)$ in τ, $O(1/\varepsilon)$ in t as long as we do not enter a ε-neighborhood of M_0. From (26), we can estimate the fast time T_1 needed to approach M_0,

$$x(0) e^{-z_0 T_1/2} \cos\left(\sqrt{4 - z_0^2}\, \frac{T_1}{2}\right) = \varepsilon. \tag{27}$$

Ignoring the oscillations, a rough estimate is

$$T_1 \approx -\frac{2}{z_0} \ln\left(\frac{\varepsilon}{x_0}\right). \tag{28}$$

The approximate time needed for the motion until $z = 0$ along M_0 is $T_2 = z_0/(\varepsilon a_0)$. Using the R-symmetry for system (4) (Subsection II B), we find the estimate of the return time $T \geq 2(T_1 + T_2)$ of the flow. The pulse-like behavior for the fast motion of the flow is shown in Fig. 23. The solutions of the slow–fast system will traverse an $O(\sqrt{\varepsilon})$ neighborhood of the origin spending the same time for positive and negative values of z.

Geometric singular perturbation theory in combination with time reversal and symmetry produces the behavior shown in the Poincaré maps of Fig. 1. Increasing ε we expect the tori to break up, maybe with Cantor gaps as in near-integrable Hamiltonian systems. In Ref. 6, it was shown by the SDDS NAFF algorithm of Ref. 7 that in the tori region, we can locate an accumulation of frequencies of the quasi-periodic and periodic solutions on the tori producing loss of regularity of the frequency map. This is carried out by looking for quasi- periodic and periodic solutions on the tori and identifying by Fourier analysis the relevant periods of the solutions. After constructing the frequency map, this yields chaotic motion between the tori. The analysis carries over to the Sprott AB system.

IX. DISCUSSION AND CONCLUSIONS

1. The Sprott B system is an important addition to the thermostatic systems proposed in Ref. 1. The thermostatic control involves the energy of the controlled system.

2. The Sprott B system shows the same reversal symmetry as systems Sprott A and NE9 leading to application of dissipative KAM theory.

3. Because of the unusual presence of an exact 2π-periodic solution for all positive values of the parameter a, we can explore the phenomena arising in the infinite many instability intervals of the exact solution.

4. A wealth of information arises from exploring these instability intervals. This leads to the discovery of families of periodic solutions, isolated tori corresponding with quasi-periodic solutions and strange attractors. The type of bifurcation depends on the value of the parameter a.

5. For large values of a, we find slow–fast dynamics with a family of non-hyperbolic slow manifolds causing irregular fiber oscillations.

6. We note that there is a natural generalization from Sprott B to Sprott AB by adding one parameter. Near the z axis system, Sprott AB shows again the presence of a family of tori and canard behavior. Its dynamics might be useful for applications, it can be a subject of future papers.

AUTHOR DECLARATIONS

Conflict of Interest

The authors have no conflicts to disclose.

Author Contributions

Ferdinand Verhulst: Conceptualization (equal); Formal analysis (equal); Writing – original draft (equal). **Taoufik Bakri:** Conceptualization (equal); Formal analysis (equal); Writing – original draft (equal).

DATA AVAILABILITY

The data that support the findings of this study are available from the corresponding author upon reasonable request.

REFERENCES

[1]S. Jafari, J. C. Sprott, and S. Golpayegani, "Elementary quadratic chaotic flows with no equilibria," Phys. Lett. A **377**, 699–702 (2013).

[2]J. C. Sprott, "Some simple chaotic flows," Phys. Rev. E **50**, R647–R650 (1994).

[3]V. I. Arnold, V. V. Kozlov, and A. I. Neihstadt, "Mathematical aspects of classical and celestial mechanics," in *Encyclopaedia of Mathematical Sciences*, Dynamical Systems III, edited by V. I. Arnold (Springer, 1988).

[4]M. Messias and A. C. Reinol, "On the formation of hidden chaotic attractors and nested invariant tori in the Sprott A system," Nonlinear Dyn. **88**, 807–821 (2017).

[5]M. Messias and A. C. Reinol, "On the existence of periodic orbits and KAM tori in the Sprott A system: A special case of the Nosé-Hoover oscillator," Nonlinear Dyn. **92**, 1287–1297 (2018).

[6]T. Bakri and F. Verhulst, "Time-reversal, tori families and canards in the Sprott A and NE9 systems," Chaos **32**, 083119 (2022).

[7]J. Laskar, "Frequency analysis of a dynamical system," Celest. Mech. Dyn. Astron. **56**, 191–196 (1993).

[8]M. E. Tuckerman, *Statistical Mechanics: Theory and Molecular Simulation*, 2nd ed. (Oxford University Press, 2010).

[9]E. Doedel, A. R. Champneys, T. F. Fairgrieve, Y. A. Kuznetsov, B. Sandstede, and X. J. Wang, *AUTO97: Continuation and bifurcation software for ordinary differential equations (with Hom-Cont)*, silver ed. (Concordia University, Montreal, 1997). Download versions at GifHub and SourceForge.

[10]Matcont, see http://www.matcont.ugent.be for "Numerical Continuation and Bifurcation Program."

[11]J. A. G. Roberts and G. R. W. Quispel, "Chaos and time-reversal symmetry. Order and chaos in reversible dynamical systems," Phys. Rep. **216**, 63–177 (1992).

[12]M.-C. Ciocci, A. Litvak-Hinenzon, and H. W. Broer, "Survey on dissipative KAM theory including quasi-periodic bifurcation theory," in *Geometric Mechanics and Symmetry: The Peyresq Lectures* (London Mathematical Society, 2005), Vol. 306, pp. 303–355.

[13]J. S. W. Lamb and J. A. G. Roberts, "Time-reversal symmetry in dynamical systems: A survey," Physica D **112**, 61–39 (1998).

[14]F. Verhulst, *Nonlinear Differential Equations and Dynamical Systems*, 2nd ed. (Springer, New York, 2000).

[15]F. Verhulst, "A toolbox of averaging theorems, ordinary and partial differential equations," in *Surveys and Tutorials in the Applied Mathematical Sciences* (Springer, 2023).

[16]F. Verhulst, *Methods and Applications of Singular Perturbations* (Springer, New York, 2005).

[17]C. Simo, "On the analytical and numerical approximation of invariant manifolds," in *Modern Methods in Celestial Mechanics. Proceedings of 13th Springschool on Astrophysics* (Editions Frontières, Paris, 1989).

[18]H. Poincaré, *Les Méthodes Nouvelles de la Mécanique Céleste* (Gauthier-Villars, Paris, 1892), Vol. 3.

[19]J. A. Sanders, F. Verhulst, and J. Murdock, *Averaging Methods in Nonlinear Dynamical Systems*, rev.ed. (Springer-Verlag, 2007).

[20]A. N. Tikhonov, "Systems of differential equations containing a small parameter multiplying the derivative," Math. Sb. **31**(73), 575–586 (1952) (in Russian).

08 October 2024 08:33:54